



Longitudinal asymmetry and its effect on pseudorapidity distributions in Pb–Pb collisions at $\sqrt{s_{\text{NN}}} = 2.76$ TeV



ALICE Collaboration*

ARTICLE INFO

Article history:

Received 30 October 2017

Received in revised form 9 March 2018

Accepted 15 March 2018

Available online 22 March 2018

Editor: L. Rolandi

ABSTRACT

First results on the longitudinal asymmetry and its effect on the pseudorapidity distributions in Pb–Pb collisions at $\sqrt{s_{\text{NN}}} = 2.76$ TeV at the Large Hadron Collider are obtained with the ALICE detector. The longitudinal asymmetry arises because of an unequal number of participating nucleons from the two colliding nuclei, and is estimated for each event by measuring the energy in the forward neutron-Zero-Degree-Calorimeters (ZNs). The effect of the longitudinal asymmetry is measured on the pseudorapidity distributions of charged particles in the regions $|\eta| < 0.9$, $2.8 < \eta < 5.1$ and $-3.7 < \eta < -1.7$ by taking the ratio of the pseudorapidity distributions from events corresponding to different regions of asymmetry. The coefficients of a polynomial fit to the ratio characterise the effect of the asymmetry. A Monte Carlo simulation using a Glauber model for the colliding nuclei is tuned to reproduce the spectrum in the ZNs and provides a relation between the measurable longitudinal asymmetry and the shift in the rapidity (y_0) of the participant zone formed by the unequal number of participating nucleons. The dependence of the coefficient of the linear term in the polynomial expansion, c_1 , on the mean value of y_0 is investigated.

© 2018 The Author(s). Published by Elsevier B.V. This is an open access article under the CC BY license (<http://creativecommons.org/licenses/by/4.0/>). Funded by SCOAP³.

1. Introduction

In a heavy-ion collision, the number of nucleons participating from each of the two colliding nuclei is finite, and will fluctuate event-by-event. The kinematic centre of mass of the participant zone, defined as the overlap region of the colliding nuclei, in general has a finite momentum in the nucleon–nucleon centre of mass frame because of the unequal number of nucleons participating from the two nuclei. This momentum causes a longitudinal asymmetry in the collision and corresponds to a shift of rapidity of the participant zone with respect to the nucleon–nucleon centre of mass (CM) rapidity, termed the rapidity-shift y_0 . The value of y_0 is indicative of the magnitude of the longitudinal asymmetry of the collision [1,2]. Assuming the number of nucleons participating from each of the two nuclei is A and B , the longitudinal asymmetry in participants is defined as $\alpha_{\text{part}} = \frac{A-B}{A+B}$ and the rapidity-shift can be approximated as $y_0 \cong \frac{1}{2} \ln \frac{A}{B}$ at LHC energies [2].

The shift in the CM frame of the participant zone, which evolves into a state of dense nuclear matter, needs to be explored in heavy-ion collision models. Comparison of model predictions with the observed Λ -polarisation, possibly due to vorticity from the initial state angular momentum surviving the evolution, requires a precise determination of initial conditions and hence the

shift in the CM frame [3–5]. Such a shift may also affect observations on correlations amongst particles, which eventually provide information about the state of the matter through model comparisons. Further, the resultant decrease in the CM energy may affect various observables including the particle multiplicity. The transverse spectra are known to be affected by the initial geometry of the events, as estimated through techniques of event shape engineering, indicating an interplay between radial and transverse flow [6]. The measurement of longitudinal asymmetry will provide a new parameter towards event shape engineering, affecting many other observables.

The simplest of all possible investigations into the effect of longitudinal asymmetry is a search for modification of the kinematic distribution of the particles. The pseudorapidity distribution ($dN/d\eta$) of soft particles, averaged over a large number of events, is symmetric in collisions of identical nuclei. These distributions were observed to be asymmetric in collisions of unequal nuclei such as d–Au [7] and p–Pb [8–10] and have been explained in terms of the rapidity-shift of the participant zone [11]. In a heavy-ion collision, the effect of the rapidity-shift of the participant zone should be discernible in the distribution of produced particles. This small effect can be estimated by taking the ratio of pseudorapidity distributions in events corresponding to different longitudinal asymmetries [2].

It was suggested that the rapidity distribution of an event, scaled by the average rapidity distribution, can be expanded in terms of Chebyshev polynomials, where the coefficients of expansion

* E-mail address: alice-publications@cern.ch.

sion are measures of the strength of longitudinal fluctuations and can be determined by measuring the two particle correlation function [12]. Using the same methodology, the event-by-event pseudorapidity distributions are also expanded in terms of Legendre polynomials [13]. The ATLAS Collaboration expanded the pseudorapidity distributions in terms of Legendre polynomials and obtained the coefficients by studying pseudorapidity correlations [14].

In the present work, the events are classified according to the asymmetry determined from the measurement of energies of neutron spectators on both sides of the collision [2]. The effect of asymmetry is investigated by taking the ratio of the measured raw $dN/d\eta$ distributions for events from different regions of the distribution of measured asymmetry. A major advantage of studying this ratio is the cancellation of (i) systematic uncertainties and (ii) the effects of short range correlations. The first measurements of the effect of asymmetry on the raw $dN/d\eta$ distributions are reported here.

The paper is organised as follows: Sect. 2 provides an introduction to the experimental setup and the details of the data sample. Section 3 discusses the characterisation of the change in raw $dN/d\eta$ distributions for events classified in different asymmetry regions. Section 4 describes the simulations employed to provide a relation between the measured asymmetry and the rapidity-shift y_0 of the participant zone. The relation between the parameter characterising the change in raw $dN/d\eta$ distributions is shown for different centralities in Sect. 5, along with its relation to the estimated values of y_0 .

2. Experimental details and data sample

The analysis uses data from Pb–Pb collision events at $\sqrt{s_{NN}} = 2.76$ TeV, recorded in the ALICE experiment in 2010, with a minimum bias trigger [15,16]. The data used in the present analysis is recorded in the neutron Zero Degree Calorimeters (ZNs), the V0 detectors, the Time Projection Chamber (TPC) and the Inner Tracking System (ITS). Both ZNs and V0 detectors are on either side of the interaction vertex, those in the direction of positive pseudorapidity axis are referred as V0A and ZNA and those in the opposite direction are referred as V0C and ZNC. A detailed description of the ALICE detectors and their performance can be found elsewhere [17, 18].

The event asymmetry is estimated using the energy measured in the two ZNs situated 114 metres away from the nominal interaction point (IP) on either side. The ZNs detect only spectator neutrons that are not bound in nuclear fragments, since the latter are bent away by the magnetic field of the LHC separation dipole. The ZN detection probability for neutrons is $97.0\% \pm 0.2\%$ (stat) $\pm 3\%$ (syst) [19]. The relative energy resolution of the $1n$ peak at 1.38 TeV is 21% for the ZNA and 20% for the ZNC [19]. The production of nuclear fragments increases with collision impact parameter degrading the resolution on the number of participating nucleons. The energy in the ZNs is a good measure of the number of spectator neutrons only for the more central collisions [18]. The analysis is limited to the top 35% most central sample and employs data from ~ 2.7 million events.

The raw $dN/d\eta$ distributions in the region $|\eta| < 0.9$ are obtained by reconstructing the charged particle tracks using the TPC and ITS. The requirements on the reconstructed tracks obtained using the measurements in these detectors are the same as in other earlier analyses [15]. The measured amplitudes in the V0A ($+2.8 < \eta < +5.1$) and V0C ($-3.7 < \eta < -1.7$) are used to estimate the raw $dN/d\eta$ distributions of charged particles in the forward regions. Both V0A and V0C are scintillator counters, each with four segments in pseudorapidity and eight segments in azimuth. The raw distributions measured are termed as $dN/d\eta$ dis-

tributions throughout the manuscript. In order to ensure a uniform detector performance, the present analysis uses events with z position (along the beam direction) of the interaction vertex, V_z , within ± 5 cm of the IP in ALICE. The centrality of Pb–Pb collisions was estimated by two independent methods. One estimate was based on the charged particle multiplicity reconstructed in the TPC and the other was based on the amplitudes in the V0 detectors [20].

3. Analysis and systematic uncertainties

In the present analysis, changes in the raw pseudorapidity distribution of charged particles are investigated for different values of measured asymmetry of the event. The method of measurement of the asymmetry and the parameters characterising the change in $dN/d\eta$ distributions are discussed in this section.

3.1. Analysis

Any event asymmetry due to unequal number of nucleons from the two participating nuclei may manifest itself in the longitudinal distributions, i.e. dN/dy (or $dN/d\eta$) of the produced particles because of a shift in the effective CM. Assuming that the rapidity distributions can be described by a symmetric function about a mean y_0 ($y_0 = 0.0$ for symmetric events), the ratio of the distributions for asymmetric and symmetric events may be written as

$$\frac{(dN/dy)_{\text{asym}}}{(dN/dy)_{\text{sym}}} = \frac{f(y - y_0)}{f(y)} \propto \sum_{n=0}^{\infty} c_n(y_0) y^n \quad (1)$$

For any functional form of the rapidity distribution, this ratio may be expanded in a Taylor series. The coefficients c_n of the different terms in the expansion depend on the shape and the parameters of the rapidity distribution [2]. In the ALICE experiment, the pseudorapidities of the emitted particles were measured. The effect of a rapidity-shift y_0 on the pseudorapidity distribution is discussed in Sect. 4.2.

The unequal number of participating nucleons will yield a non-zero y_0 of the participant zone and will cause an asymmetry in the number of spectators. This asymmetry can provide information about the mean values of y_0 using the response matrix discussed in Sect. 4. The asymmetry of each event is estimated by measuring the energy in the ZNs on both sides of the interaction vertex: E_{ZNA} on the side referred to as the A-side ($\eta > 0$) and E_{ZNC} on the side referred to as the C-side ($\eta < 0$). A small difference in the mean and the relative energy resolution of the $1n$ peak at 1.38 TeV was observed in the performance of the two ZNs [19]. For each centrality interval, the energy distribution in each ZN is divided by its mean, and the width of the $E_{\text{ZNC}}/\langle E_{\text{ZNC}} \rangle$ distribution is scaled to the width of the corresponding distribution using E_{ZNA} . The asymmetry in ZN is defined as

$$\alpha_{\text{ZN}} = \frac{\varepsilon_{\text{ZNA}} - \varepsilon_{\text{ZNC}}}{\varepsilon_{\text{ZNA}} + \varepsilon_{\text{ZNC}}} \quad (2)$$

where $\varepsilon_{\text{ZNC(A)}}$ is a dimensionless quantity for each event, obtained after scaling the distributions of $E_{\text{ZNC(A)}}$ as described above.

For the 15–20% centrality interval, Fig. 1 shows the distribution of the asymmetry α_{ZN} . To investigate the significance of this distribution, the contribution of the resolution of ZNs to the resolution of the asymmetry parameter α_{ZN} is evaluated. For each centrality interval, values of E_{ZNC} and E_{ZNA} are simulated for each event by assuming a normal distribution peaked at the mean value

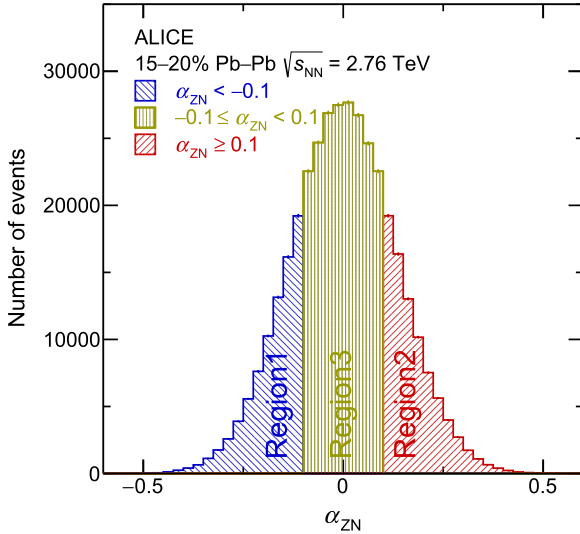


Fig. 1. The distribution of the asymmetry parameter α_{ZN} for the 15–20% centrality interval. The distribution is demarcated into three regions using $|\alpha_{ZN}^{\text{cut}}|$. A Gaussian fit to the distribution yields a width of 0.13.

corresponding to the average number of neutrons and the corresponding energy resolution. The average number of neutrons is estimated by dividing the experimental distribution of energy in ZN by 1.38 TeV. These values are used to obtain α_{ZN} for each event and its distribution. The width of the distribution corresponds to the intrinsic resolution of the measured parameter α_{ZN} and varies from 0.023 to 0.050 from the most peripheral (30–35%) selection to the most central (0–5%) selection. The observed width of 0.13 of the distribution of α_{ZN} reported in Fig. 1 is considerably larger than the resolution of α_{ZN} (0.027 for the centrality interval corresponding to the data in the figure) and the increase in width may be attributed to the event-by-event fluctuations in the number of neutrons detected in each ZN. To investigate the effect of α_{ZN} on the $dN/d\eta$ distributions, the events are demarcated into three regions of asymmetry by choosing a cut value α_{ZN}^{cut} . These regions correspond to (i) $\alpha_{ZN} < -\alpha_{ZN}^{\text{cut}}$ (Region 1), (ii) $\alpha_{ZN} \geq \alpha_{ZN}^{\text{cut}}$ (Region 2) and (iii) $-\alpha_{ZN}^{\text{cut}} \leq \alpha_{ZN} < \alpha_{ZN}^{\text{cut}}$ (Region 3). Regions 1 and 2 are referred to as the asymmetric regions and Region 3 is referred to as the symmetric region.

The effect of the measured asymmetry α_{ZN} on the pseudorapidity distributions is investigated by studying the ratio of $dN/d\eta$ distribution in events from the asymmetric region to those from the symmetric region. There are small differences in the distributions of centrality and vertex position in events of different regions of asymmetry. It is necessary to ensure that any correlation between the ratio of $dN/d\eta$ and the asymmetry is not due to a systematic effect of a shift in the interaction vertex. To eliminate any possible systematic bias on the measured distributions, the $dN/d\eta$ distributions are corrected by weight factors obtained by normalising the number of events in asymmetric and symmetric regions in each 1% centrality interval and each 1 cm range of vertex positions.

For the 15–20% centrality interval, the distributions of these factors in the two cases corresponding to the asymmetry regions 1 and 2 have a mean of 1.0 and an rms of 0.05 and 0.06 respectively. The weight factors do not show any systematic dependence on the position of the vertex. This is expected considering the large distance between the ZNs as compared to variations in the vertex position. The factors show a systematic dependence on 1% centrality bins within each centrality interval. The 1% centrality bin with the greater number of participants tends to have more asymmetric events, presumably to compensate for the decrease in the effective CM energy due to the motion of the participant zone; the weight

factor is 1.08 for the most central 15–16% centrality bin and is 0.94 for the 19–20% centrality bin.

The ratio of $dN/d\eta$ for events corresponding to different regions of asymmetry, as shown in Fig. 1, is determined. For $|\eta| < 1.0$, the ratio is obtained using $dN/d\eta$ for tracks. For $|\eta| > 1.0$, the ratio shown in Fig. 2 (a) and (b) is obtained from amplitudes measured in VOA and the one shown in Fig. 2(c) and (d) is from amplitudes measured in VOC. The squares in Fig. 2 (a) and (c) represent the ratio of $dN/d\eta$ in the asymmetry Region 1 to that in Region 3 (R13), and the stars represent the corresponding ratio in Region 2 to Region 3 (R23). The filled circles in Fig. 2 (b) and (d) are obtained by (i) reflecting the data points labelled R23 across $\eta = 0$ and (ii) taking the averages of R13 and reflected-R23 for $|\eta| < 1.0$. A third order polynomial is fitted to the points and the values of the coefficients c_n along with the χ^2 are shown. The polynomial fit to the ratio of $dN/d\eta$ distribution has a dominantly linear term. A small residual detector effect is observed when determining c_1 using data measured in VOA and when using data measured in VOC. In all subsequent discussion, the values of c_1 quoted are the mean of values obtained from the measurements in VOA and VOC.

Considering that the event samples corresponding to different regions of asymmetry are identical in all aspects other than their values of measured α_{ZN} , the observation of non-zero values of c_1 can be attributed to the asymmetry. For a fixed centrality interval, c_1 depends on the choice of α_{ZN}^{cut} . The analysis is repeated for different values of α_{ZN}^{cut} and the dependence of c_1 on α_{ZN}^{cut} is shown in Fig. 3, for different centralities. For each centrality interval the coefficient c_1 has a linear dependence on α_{ZN}^{cut} and the slope increases with decreasing centrality; c_1 increases for events corresponding to larger values of average event asymmetry. The range of values of α_{ZN}^{cut} was guided by the resolution and the width of the distribution of α_{ZN} , as mentioned in reference to Fig. 1. Increasing the value of α_{ZN}^{cut} increases the mean $\langle \alpha_{ZN} \rangle$ for events from the asymmetric class (Region 1 or Region 2), and increases the RMS of α_{ZN} for events from the symmetric class (Region 3).

3.2. Systematic uncertainties

The current method of analysis uses the ratio of two $dN/d\eta$ distributions from events divided on the basis of measurements in ZNs, within a centrality interval. All effects due to limited efficiency, acceptance or contamination would cancel while obtaining the value of the ratio. The contributions to the systematic uncertainties on c_1 are estimated due to the following sources:

1. Centrality selection: the ratio of $dN/d\eta$ is obtained from the measurements of tracks in the ITS+TPC at midrapidity and charge particle signal amplitudes in the VO at forward rapidities. For the former, the event centrality is determined using the measurements in the VO and for the latter using the track multiplicity in the TPC. The analysis is repeated by interchanging the centrality criteria and the resultant change in the values of c_1 for different centrality intervals is in the range 0.1% to 3.6%.
2. VOA and VOC: the systematic uncertainty on the mean value of c_1 is estimated by assuming a uniform probability distribution for the correct value of c_1 to lie between the two values obtained using the charged-particle signal amplitudes measured in the VOA and the VOC. The uncertainty is in the range 2.1% to 4.6% and does not depend on the centrality value.
3. Vertex position: the analysis is repeated for the z position of the interaction vertex $|V_z| \leq 3.0$ cm. For the most central interval, the results change by less than 0.1%. For the 15–20%

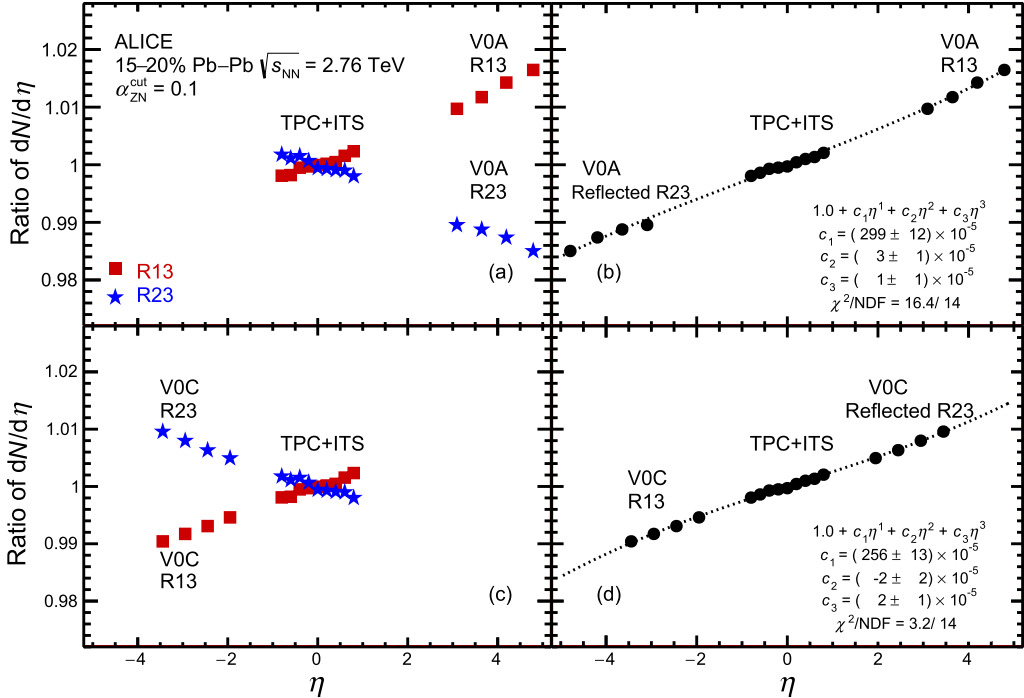


Fig. 2. The ratio of $dN/d\eta$ distribution for events from the different regions of α_{ZN} distribution of Fig. 1. The $dN/d\eta$ distributions are obtained as described in Sect. 2. (a) The square (star) symbols corresponding to R13 (R23) are obtained by taking the ratio of $dN/d\eta$ of events from Region 1 (Region 2) to Region 3. (b) The data points are obtained after reflection across $\eta = 0$ as described in the text. The data for $|\eta| > 1.0$ in panels (a) and (b) are from measurements in VOA and in panels (c) and (d) are from measurements in V0C.

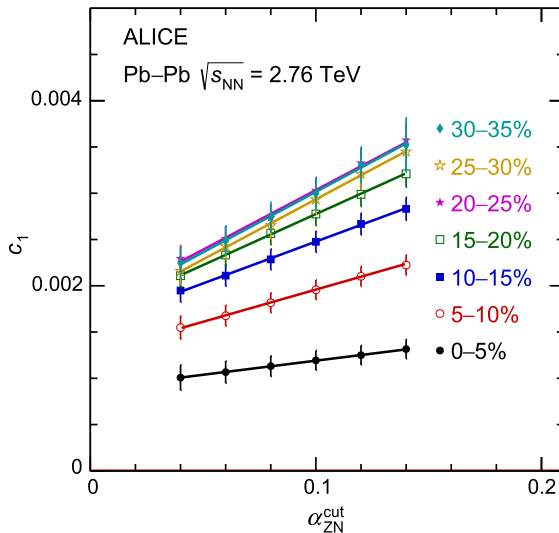


Fig. 3. The coefficient c_1 characterising the change in $dN/d\eta$ distribution for asymmetric regions is shown for different values of α_{ZN}^{cut} (α_{ZN}^{cut} demarcates the asymmetric and symmetric events) for each centrality interval.

centrality interval, the results change by 3.3% and for all other centrality intervals, the changes are less than 1.3%.

4. Weight factors for normalisation: the analysis is also repeated without the weight factors mentioned in Sect. 3.1 for the centrality and the vertex normalisation in the number of events. The change in the results is 4.9% in the most central class and less than 1% for all other centrality intervals.

The total systematic uncertainty is obtained by adding the four uncertainties in quadrature. The resultant uncertainty is in the range 2.3% to 5.8% and is shown by the band in Fig. 8.

4. Simulations

The simulation used for obtaining a relation between rapidity-shift y_0 and the measurable asymmetry α_{ZN} is described in this section. This simulation has three components: (i) a Glauber Monte Carlo to generate number of participants and spectator protons and neutrons, (ii) a function parametrised to fit the average loss of spectator neutrons due to spectator fragmentation (the loss of spectator neutrons in each event is smeared around this average) and (iii) the response of the ZN to single neutrons. The simulation encompassing the above is referred to in the present work as Tuned Glauber Monte Carlo (TGMC), and reproduces the energy distributions in the ZNs. The effect of y_0 on the pseudorapidity distributions has been estimated using additional simulations for a Gaussian dN/dy and are also described in this section.

4.1. Asymmetry and rapidity-shift

The Glauber Monte Carlo model [21] used in the present work assumes a nucleon–nucleon interaction cross section of 64 mb at $\sqrt{s_{NN}} = 2.76$ TeV. The model yields the number of participating nucleons in the overlap zone from each of the colliding nuclei. The range of impact parameters for each 5% centrality interval is taken from our Pb–Pb centrality paper [20]. For each centrality interval, 0.4 million events are generated.

For each generated event, the number of participating protons and neutrons is obtained, enabling a determination of the rapidity-shift y_0 and the various longitudinal asymmetries. If A and B are the number of spectators (spectator neutrons) in the two colliding nuclei, the asymmetry is referred to as α_{spec} ($\alpha_{spec-neut}$). Fig. 4 (a) shows the correspondence between y_0 and α_{part} . Figs. 4 (b) and (c) show the relation between y_0 and α_{spec} and $\alpha_{spec-neut}$ respectively [2]. These figures show that the rapidity-shift y_0 can be estimated by measuring α_{spec} or $\alpha_{spec-neut}$ in any experiment that uses Zero Degree Calorimeters. However, the lack of information

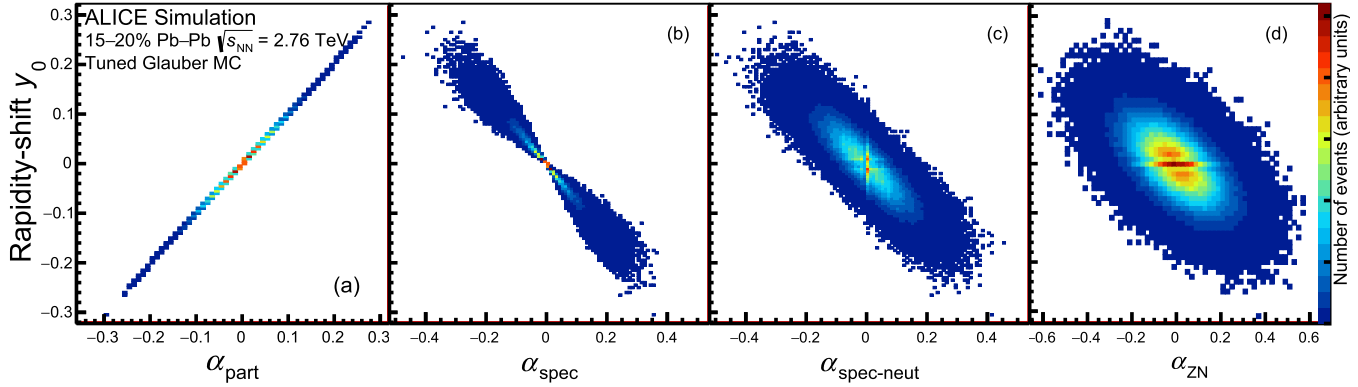


Fig. 4. Rapidity-shift y_0 as a function of asymmetry in (a) number of participants, (b) number of spectators, (c) number of spectator neutrons and (d) energy in ZN obtained using TGMC as described in the text. The results in all four panels are shown for the 15–20% centrality interval.

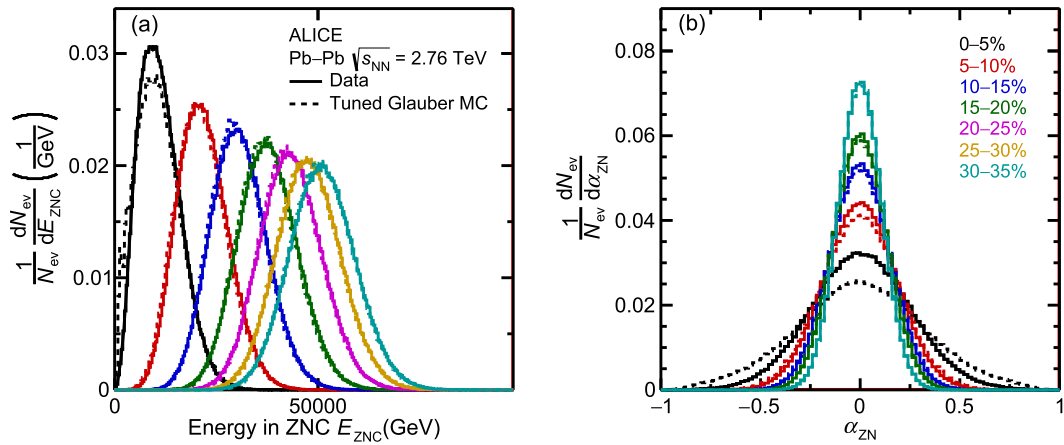


Fig. 5. (a) Distribution of energy in ZNC in each 5% centrality interval for events simulated using TGMC and for the experimental data. The peak of the distribution shifts to smaller values of E_{ZNC} with increasing centrality. (b) Distribution of the asymmetry parameter α_{ZN} in the simulated events and in experimental data for different centralities. The width of the distribution increases with increasing centrality. For clarity, only 5 distributions are shown. The distributions corresponding to 20–25% and 25–30% lie between those of 15–20% and 30–35%.

on the number of participants worsens the precision in determining y_0 . Fig. 4 (d) shows the relation between y_0 and α_{ZN} obtained in TGMC, as described in the next paragraph.

The Glauber Monte Carlo is tuned to describe the experimental distributions of ZN energy. For each 1% centrality interval, the mean number of spectator neutrons (N_s) is obtained in the Glauber Monte Carlo. Folding the ZN response yields the simulated values of mean energy as a function of centrality. The experimentally measured mean energy in the ZN is also determined for each 1% centrality interval. The ratio of the measured value of mean energy to the simulated value of mean energy gives the fractional loss (f) of neutrons due to spectator fragments that veer away due to the magnetic field. The value of f for the 0–5% centrality interval is 0.19. For all other centralities it varies from 0.40 for 5–10% to 0.55 for 30–35% centrality interval. A fluctuation proportional to the number of remaining neutrons ($N_s \times (1 - f)$) is incorporated to reproduce the experimental distribution of the energy deposited in the ZN shown in Fig. 5 (a). The peak and the RMS of the energy distributions match well. The fractional difference in the position of the peak varies between 3.7% for the 0–5% centrality interval and 0.1% for the 30–35% centrality interval. The fractional difference in RMS for the most central class is 8.6% and is in the range 1.0–2.0% for all other centrality intervals. The distributions of the asymmetry parameter for the TGMC events and the measured data for each centrality interval are shown in Fig. 5 (b). The TGMC con-

tains information of y_0 and α_{ZN} for each event. A scatter plot between y_0 and α_{ZN} is shown in Fig. 4 (d) for the 15–20% centrality interval. This constitutes the response matrix. For any measured value of α_{ZN} , the distribution of y_0 can be obtained. Any difference in the experimental and TGMC distributions of α_{ZN} can be accounted for by scaling the y_0 distribution by the ratio of number of events in data to the number in TGMC as

$$f(y_0, \alpha_{ZN}^{\text{Data}}) = f(y_0, \alpha_{ZN}^{\text{TGMC}}) \frac{N_{\text{events}}^{\text{Data}}}{N_{\text{events}}^{\text{TGMC}}}, \quad (3)$$

with Data (TGMC) in the superscript of number of events, N_{events} , denoting the experimental data (TGMC events). For each of the three regions of asymmetry shown in Fig. 1, corresponding to a chosen value of $\alpha_{ZN}^{\text{cut}} = 0.1$, the distribution of rapidity-shift y_0 obtained using the response matrix is shown in Fig. 6. It is worth mentioning that the width of the distribution of y_0 for events from Region 3, corresponding to $-\alpha_{ZN}^{\text{cut}} \leq \alpha_{ZN} < \alpha_{ZN}^{\text{cut}}$, is comparable to the widths of the corresponding distributions from Regions 1 and 2. The effect of difference in the value of the means of the y_0 distributions is investigated in the present work.

4.2. Effect of rapidity-shift on pseudorapidity distributions

The effect of a shift in the rapidity distribution by y_0 on the measurable pseudorapidity distribution ($dN/d\eta$) is investigated using simulations. For each event, the rapidity of charged particles is

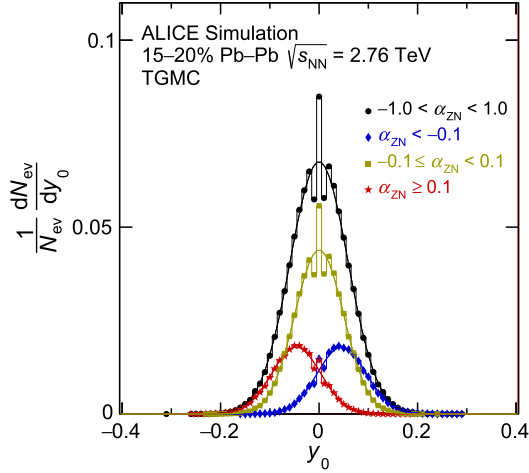


Fig. 6. The distribution of rapidity-shifts for the events from the three different regions of measured asymmetry shown in Fig. 1. Determination of y_0 uses the difference in number of nucleons. For small values of this difference, the changes in values near $y_0 = 0$ are discrete, and are smeared into a continuous distribution as y_0 increases.

generated from a Gaussian distribution of a chosen width σ_y [22]. The pseudorapidity is obtained by using the Blast-Wave model fit to the data for the transverse momentum distributions and the experimentally measured relative yields of pions, kaons and protons [23]. To simulate the effect of different widths of the parent rapidity distribution for different centralities, different σ_y widths are chosen to reproduce the measured FWHM (Full Width at Half Maximum) of the pseudorapidity distribution [24]. For the most central (0–5%) class, a value 3.86 is used for the width of the rapidity distribution, and a value 4.00 is used for the width of the least central class employed in this analysis (30–35%).

The distribution of rapidity-shift y_0 , similar to the one shown in Fig. 6, is obtained for each centrality interval and each $\alpha_{\text{ZN}}^{\text{cut}}$ using TGMC. Fig. 7 (a) shows the $\langle y_0 \rangle$ as a function of $\alpha_{\text{ZN}}^{\text{cut}}$ for different centralities. One observes a linear relation between the two quantities, showing that an asymmetry in the ZN measurement, arising from the unequal number of participating nucleons, is related to the mean rapidity-shift $\langle y_0 \rangle$. The rapidity distribution of the particles produced in each event is generated assuming a Gaussian form centred about a y_0 , which is generated randomly from the y_0 distribution. Events with a rapidity distribution shifted by

$y_0 \neq 0$ yield an asymmetric pseudorapidity distribution. A third order polynomial function in η is fitted to the ratio of the simulated $dN/d\eta$ for the asymmetric region to the simulated $dN/d\eta$ for the symmetric region. The values of the coefficients in the expansion depend upon the rapidity-shift y_0 and the parameters characterising the distribution [2].

The simulations described above were repeated for different values of $\alpha_{\text{ZN}}^{\text{cut}}$ to obtain the pseudorapidity distributions for symmetric and asymmetric regions. Fitting third order polynomial functions to the ratios of the simulated pseudorapidity distributions determines the dependence of c_1 on $\alpha_{\text{ZN}}^{\text{cut}}$. Fig. 7 (b) shows that c_1 has a linear dependence on $\alpha_{\text{ZN}}^{\text{cut}}$ for each centrality interval. The difference in the slopes for different centralities is due to differences in the distributions of y_0 and to differences in the widths of the rapidity distributions.

It is important to note that the parameter c_1 , characterising the asymmetry in the pseudorapidity distribution, shows a linear dependence on the parameter $\alpha_{\text{ZN}}^{\text{cut}}$ in the event sample generated using TGMC and simulations for a Gaussian dN/dy , akin to the dependence of the estimated value of rapidity-shift y_0 for the same sample of events.

5. Results

The longitudinal asymmetry in a heavy-ion collision has been estimated from the difference in the energy of the spectator neutrons on both sides of the collision vertex. The effect of the longitudinal asymmetry is observed in the ratio of $dN/d\eta$ distributions corresponding to different asymmetries. The linear term in a polynomial fit to the distribution of the ratio is dominant, and is characterised by its coefficient c_1 . The centrality dependence of the coefficient c_1 for $\alpha_{\text{ZN}}^{\text{cut}} = 0.1$ is shown in Fig. 8. It is worth emphasising that the values of c_1 and hence its centrality dependence are affected by (i) the distribution of rapidity-shift y_0 for each centrality interval, (ii) the chosen value of $\alpha_{\text{ZN}}^{\text{cut}}$, as seen in Fig. 7 and (iii) the shape or the width of the parent rapidity distribution for each centrality. Fig. 8 also shows the results obtained using simulations as described in Sec. 4.2 for $\alpha_{\text{ZN}}^{\text{cut}} = 0.1$. The systematic uncertainty on the simulated event sample is estimated by (i) varying the resolution of ZNs from 20% to 30%, (ii) assuming all charged particles are pions and (iii) varying the width of the parent rapidity distribution within the range corresponding to the uncertainties on FWHM quoted in Ref. [24]. The simulated events show a good agreement with the experimental data providing cre-

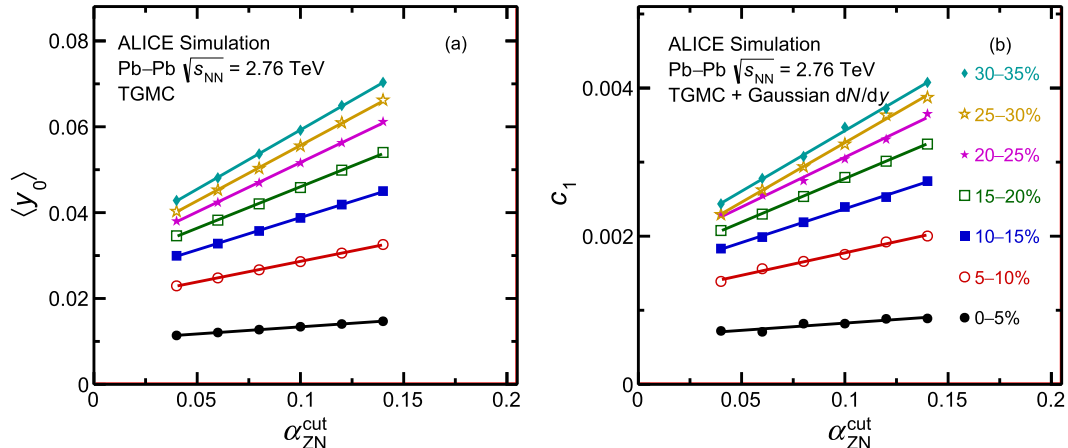


Fig. 7. (a) The estimated mean value of rapidity-shift $\langle y_0 \rangle$ for the asymmetric region characterised by different values of $\alpha_{\text{ZN}}^{\text{cut}}$ for each centrality interval. (b) The coefficient c_1 characterising the change in the pseudorapidity distributions for different values of $\alpha_{\text{ZN}}^{\text{cut}}$, for each centrality interval. These results are obtained using TGMC and simulated pseudorapidity distributions, as described in the text.

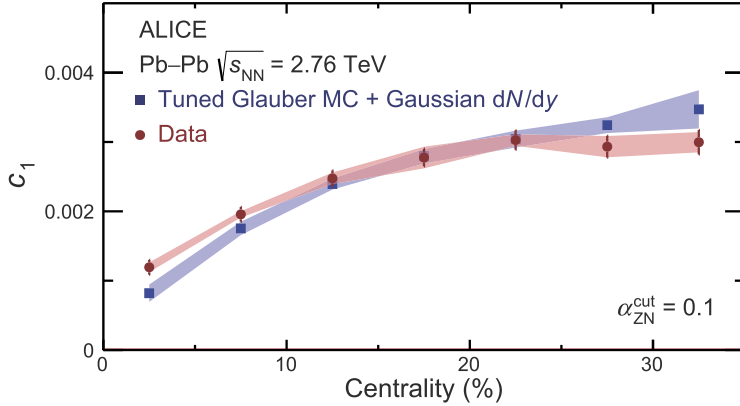


Fig. 8. The mean values of the coefficient c_1 are shown as filled circles for different centralities. These correspond to the ratio of $dN/d\eta$ distributions of populations of events demarcated by $\alpha_{ZN}^{cut} = 0.1$. The squares show the corresponding values from simulations, and correspond to $\alpha_{ZN}^{cut} = 0.1$ in Fig. 7, for different centralities. The systematic uncertainties are shown as bands.

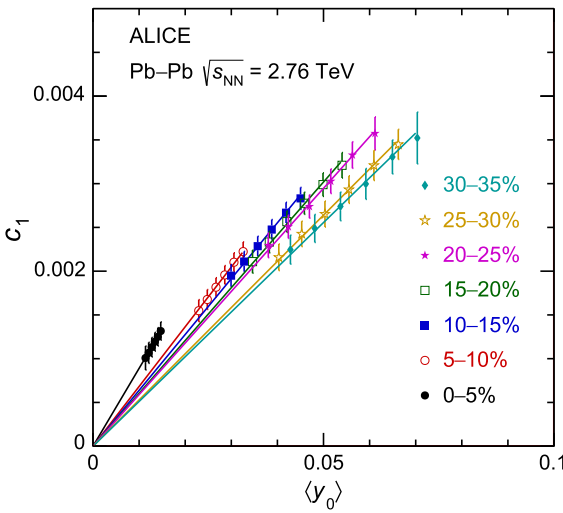


Fig. 9. For each set of events characterised by α_{ZN}^{cut} , the measured values of coefficient c_1 as a function of estimated values of mean rapidity-shift obtained using TGMC as described in the text. The results are shown for different centralities. The uncertainties for $\langle y_0 \rangle$ shown are statistical and within its symbol size. The lines are linear fits passing through the origin.

dence to the assumptions of the simulation, in particular that the asymmetry in the distributions arises from the shift of rapidity of the participant zone.

There are two quantities from independent measurements for each selection of asymmetric events. These are (i) c_1 , the parameter characterising the effect of asymmetry in the $dN/d\eta$ distributions and shown in Fig. 3 and (ii) the mean rapidity-shift $\langle y_0 \rangle$ obtained from the measured asymmetry, filtered through the corresponding response matrix (Fig. 4 (d)), and shown in Fig. 7 (a). The relation between c_1 and $\langle y_0 \rangle$ is shown in Fig. 9. The parameter c_1 shows a linear dependence on $\langle y_0 \rangle$ for each centrality. The difference in the slopes indicates the sensitivity of the longitudinal asymmetry to the details of the rapidity distribution. For a Gaussian rapidity distribution the corresponding parameter c_1 would be related to the rapidity-shift as $c_1 = \frac{y_0}{\sigma_y^2}$ [2], implying that the slope is inversely proportional to the square of the width of the distribution. The observation of an increase in the slope with an increase in the centrality in the present data indicates a decrease in the width of the pseudorapidity distribution with increasing centrality. Such a decrease in the width of the pseudorapidity distribution with increasing centrality has been observed independently by fit-

ting the pseudorapidity distributions in a broad range of pseudorapidity [24].

6. Conclusions

The present analysis demonstrates the existence of a longitudinal asymmetry in the collision of identical nuclei due to fluctuations in the number of participants from each colliding nucleus. This asymmetry has been measured in the ZNs in the ALICE experiment (Fig. 1), and affects the pseudorapidity distributions, as demonstrated by taking the ratio of distribution of events from the asymmetric region to the corresponding one from the symmetric region (Fig. 2). The effect can be characterised by the coefficient of the linear term in the polynomial expansion of the ratio. The coefficients show a linear dependence on α_{ZN}^{cut} , a parameter to classify the events into symmetric and asymmetric regions (Fig. 3). Different values of α_{ZN}^{cut} correspond to different values of the mean rapidity shift $\langle y_0 \rangle$ (Fig. 7 (a)). The parameter describing the change in the pseudorapidity distributions (c_1) has a simple explanation in the rapidity-shift $\langle y_0 \rangle$ of the participant zone (Fig. 9). The analysis confirms that the longitudinal distributions are affected by the rapidity-shift of the participant zone with respect to the nucleon-nucleon CM frame. The results provide support to the relevance of number of nucleons affecting the production of charged particles, even at such high energies.

The longitudinal asymmetry is a good variable to classify the events and provides information on the initial state of each event. A systematic study of the effects of longitudinal asymmetry on different observables, e.g. the odd harmonics of anisotropic flow, the forward-backward correlations, the source sizes, in heavy-ion collisions may reveal other characteristics of the initial state and of particle production phenomena.

Acknowledgements

The ALICE Collaboration would like to thank all its engineers and technicians for their invaluable contributions to the construction of the experiment and the CERN accelerator teams for the outstanding performance of the LHC complex. The ALICE Collaboration gratefully acknowledges the resources and support provided by all Grid centres and the Worldwide LHC Computing Grid (WLCG) collaboration. The ALICE Collaboration acknowledges the following funding agencies for their support in building and running the ALICE detector: A.I. Alikhanian National Science Laboratory (Yerevan Physics Institute) Foundation (ANSL), State Committee of Science and World Federation of Scientists (WFS), Armenia;

Austrian Academy of Sciences and Nationalstiftung für Forschung, Technologie und Entwicklung, Austria; Ministry of Communications and High Technologies, National Nuclear Research Center, Azerbaijan; Conselho Nacional de Desenvolvimento Científico e Tecnológico (CNPq), Universidade Federal do Rio Grande do Sul (UFRGS), Financiadora de Estudos e Projetos (Finep) and Fundação de Amparo à Pesquisa do Estado de São Paulo (FAPESP), Brazil; Ministry of Science & Technology of China (MSTC), National Natural Science Foundation of China (NSFC) and Ministry of Education of China (MOEC), China; Ministry of Science, Education and Sport and Croatian Science Foundation, Croatia; Ministry of Education, Youth and Sports of the Czech Republic, Czech Republic; The Danish Council for Independent Research | Natural Sciences, the Carlsberg Foundation and Danish National Research Foundation (DNRF), Denmark; Helsinki Institute of Physics (HIP), Finland; Commissariat à l’Energie Atomique (CEA) and Institut National de Physique Nucléaire et de Physique des Particules (IN2P3) and Centre National de la Recherche Scientifique (CNRS), France; Bundesministerium für Bildung, Wissenschaft, Forschung und Technologie (BMBF) and GSI Helmholtzzentrum für Schwerionenforschung GmbH, Germany; General Secretariat for Research and Technology, Ministry of Education, Research and Religious, Greece; National Research, Development and Innovation Office, Hungary; Department of Atomic Energy, Government of India (DAE), Department of Science and Technology, Government of India (DST), University Grants Commission, Government of India (UGC) and Council of Scientific and Industrial Research (CSIR), India; Indonesian Institute of Science, Indonesia; Centro Fermi – Museo Storico della Fisica e Centro Studi e Ricerche Enrico Fermi and Istituto Nazionale di Fisica Nucleare (INFN), Italy; Institute for Innovative Science and Technology, Nagasaki Institute of Applied Science (IIIST), Japan Society for the Promotion of Science (JSPS) KAKENHI and Japanese Ministry of Education, Culture, Sports, Science and Technology (MEXT), Japan; Consejo Nacional de Ciencia (CONACYT) y Tecnología, through Fondo de Cooperación Internacional en Ciencia y Tecnología (FONCICYT) and Dirección General de Asuntos del Personal Académico (DGAPA), Mexico; Nederlandse Organisatie voor Wetenschappelijk Onderzoek (NWO), Netherlands; The Research Council of Norway, Norway; Commission on Science and Technology for Sustainable Development in the South (COMSATS), Pakistan; Pontificia Universidad Católica del Perú, Peru; Ministry of Science and Higher Education and National Science Centre, Poland; Korea Institute of Science and Technology Information and National Research Foundation of Korea (NRF), Republic of Korea; Ministry of Education and Scientific Research, Institute of Atomic Physics and Romanian National Agency for Science, Technology and Innovation, Romania; Joint Institute for Nuclear Research (JINR), Ministry of Education and Science of the Russian Federation and National Research Centre Kurchatov Institute, Russia; Ministry of Education, Science, Research and Sport of the Slovak Republic, Slovakia; National Research Foundation of South Africa, South Africa; Centro de Aplicaciones Tecnológicas y Desarrollo Nuclear (CEADEN), Cubaenergía, Cuba, Ministerio de Ciencia e Innovacion and Centro de Investigaciones Energéticas, Medioambientales y Tecnológicas (CIEMAT), Spain; Swedish Research Council (VR) and Knut & Alice Wallenberg Foundation (KAW), Sweden; European Organization for Nuclear Research, Switzerland; National Science and Technology Development Agency (NSDTA), Suranaree University of Technology (SUT) and Office of the Higher Education Commission under NRU project of Thailand, Thailand; Turkish Atomic Energy Agency (TAEK), Turkey; National Academy of Sciences of Ukraine, Ukraine; Science and Technology Facilities Council (STFC), United Kingdom; National Science Foundation of the United States of America (NSF)

and United States Department of Energy, Office of Nuclear Physics (DOE NP), United States of America.

References

- [1] V. Vovchenko, D. Anchishkin, L.P. Csernai, Longitudinal fluctuations of the center of mass of the participants in heavy-ion collisions, *Phys. Rev. C* **88** (1) (2013) 014901, arXiv:1306.5208 [nucl-th].
- [2] R. Raniwala, S. Raniwala, C. Loizides, Effects of longitudinal asymmetry in heavy-ion collisions, *Phys. Rev. C* **97** (2) (2018) 024912, arXiv:1608.01428 [nucl-ex].
- [3] STAR Collaboration, L. Adamczyk, et al., Global Λ hyperon polarization in nuclear collisions: evidence for the most vortical fluid, *Nature* **548** (2017) 62–65, arXiv:1701.06657 [nucl-ex].
- [4] F. Becattini, L. Csernai, D.J. Wang, A polarization in peripheral heavy ion collisions, *Phys. Rev. C* **88** (3) (2013) 034905, arXiv:1304.4427 [nucl-th]; Erratum *Phys. Rev. C* **93** (6) (2016) 069901.
- [5] Y. Xie, D. Wang, L.P. Csernai, Global Λ polarization in high energy collisions, *Phys. Rev. C* **95** (3) (2017) 031901, arXiv:1703.03770 [nucl-th].
- [6] ALICE Collaboration, J. Adam, et al., Event shape engineering for inclusive spectra and elliptic flow in Pb–Pb collisions at $\sqrt{s_{NN}} = 2.76$ TeV, *Phys. Rev. C* **93** (3) (2016) 034916, arXiv:1507.06194 [nucl-ex].
- [7] PHOBOS Collaboration, B.B. Back, et al., Pseudorapidity distribution of charged particles in d + Au collisions at $s(NN)^{1/2} = 200$ -GeV, *Phys. Rev. Lett.* **93** (2004) 082301, arXiv:nucl-ex/0311009.
- [8] ALICE Collaboration, B. Abelev, et al., Pseudorapidity density of charged particles in p + Pb collisions at $\sqrt{s_{NN}} = 5.02$ TeV, *Phys. Rev. Lett.* **110** (3) (2013) 032301, arXiv:1210.3615 [nucl-ex].
- [9] ALICE Collaboration, J. Adam, et al., Centrality dependence of particle production in p-Pb collisions at $\sqrt{s_{NN}} = 5.02$ TeV, *Phys. Rev. C* **91** (6) (2015) 064905, arXiv:1412.6828 [nucl-ex].
- [10] ATLAS Collaboration, G. Aad, et al., Measurement of the centrality dependence of the charged-particle pseudorapidity distribution in proton-lead collisions at $\sqrt{s_{NN}} = 5.02$ TeV with the ATLAS detector, *Eur. Phys. J. C* **76** (4) (2016) 199, arXiv:1508.00848 [hep-ex].
- [11] P. Steinberg, Inclusive pseudorapidity distributions in p(d) + A collisions modeled by shifted rapidity distributions, *Phys. Lett. B* (2007), submitted for publication, arXiv:nucl-ex/0703002.
- [12] A. Bzdak, D. Teaney, Longitudinal fluctuations of the fireball density in heavy-ion collisions, *Phys. Rev. C* **87** (2) (2013) 024906, arXiv:1210.1965 [nucl-th].
- [13] J. Jia, S. Radhakrishnan, M. Zhou, Forward-backward multiplicity fluctuation and longitudinal harmonics in high-energy nuclear collisions, *Phys. Rev. C* **93** (4) (2016) 044905, arXiv:1506.03496 [nucl-th].
- [14] ATLAS Collaboration, M. Aaboud, et al., Measurement of forward-backward multiplicity correlations in lead-lead, proton-lead, and proton-proton collisions with the ATLAS detector, *Phys. Rev. C* **95** (6) (2017) 064914, arXiv:1606.08170 [hep-ex].
- [15] ALICE Collaboration, K. Aamodt, et al., Elliptic flow of charged particles in Pb–Pb collisions at 2.76 TeV, *Phys. Rev. Lett.* **105** (2010) 252302, arXiv:1011.3914 [nucl-ex].
- [16] ALICE Collaboration, K. Aamodt, et al., Centrality dependence of the charged-particle multiplicity density at mid-rapidity in Pb–Pb collisions at $\sqrt{s_{NN}} = 2.76$ TeV, *Phys. Rev. Lett.* **106** (2011) 032301, arXiv:1012.1657 [nucl-ex].
- [17] ALICE Collaboration, K. Aamodt, et al., The ALICE experiment at the CERN LHC, *J. Instrum.* **3** (2008) S08002.
- [18] ALICE Collaboration, B.B. Abelev, et al., Performance of the ALICE experiment at the CERN LHC, *Int. J. Mod. Phys. A* **29** (2014) 1430044, arXiv:1402.4476 [nucl-ex].
- [19] ALICE Collaboration, B. Abelev, et al., Measurement of the cross section for electromagnetic dissociation with neutron emission in Pb–Pb collisions at $\sqrt{s_{NN}} = 2.76$ TeV, *Phys. Rev. Lett.* **109** (2012) 252302, arXiv:1203.2436 [nucl-ex].
- [20] ALICE Collaboration, B. Abelev, et al., Centrality determination of Pb–Pb collisions at $\sqrt{s_{NN}} = 2.76$ TeV with ALICE, *Phys. Rev. C* **88** (4) (2013) 044909, arXiv:1301.4361 [nucl-ex].
- [21] B. Alver, M. Baker, C. Loizides, P. Steinberg, The PHOBOS Glauber Monte Carlo, arXiv:0805.4411 [nucl-ex].
- [22] ALICE Collaboration, E. Abbas, et al., Centrality dependence of the pseudorapidity density distribution for charged particles in Pb–Pb collisions at $\sqrt{s_{NN}} = 2.76$ TeV, *Phys. Lett. B* **726** (2013) 610–622, arXiv:1304.0347 [nucl-ex].
- [23] ALICE Collaboration, B. Abelev, et al., Centrality dependence of π , K, p production in Pb–Pb collisions at $\sqrt{s_{NN}} = 2.76$ TeV, *Phys. Rev. C* **88** (2013) 044910, arXiv:1303.0737 [hep-ex].
- [24] ALICE Collaboration, J. Adam, et al., Centrality evolution of the charged-particle pseudorapidity density over a broad pseudorapidity range in Pb–Pb collisions at $\sqrt{s_{NN}} = 2.76$ TeV, *Phys. Lett. B* **754** (2016) 373–385, arXiv:1509.07299 [nucl-ex].

ALICE Collaboration

- S. Acharya ¹³⁷, J. Adam ⁹⁶, D. Adamová ⁹³, J. Adolfsson ³², M.M. Aggarwal ⁹⁸, G. Aglieri Rinella ³³, M. Agnello ²⁹, N. Agrawal ⁴⁶, Z. Ahammed ¹³⁷, N. Ahmad ¹⁵, S.U. Ahn ⁷⁸, S. Aiola ¹⁴¹, A. Akindinov ⁶³, M. Al-Turany ¹⁰⁶, S.N. Alam ¹³⁷, J.L.B. Alba ¹¹¹, D.S.D. Albuquerque ¹²², D. Aleksandrov ⁸⁹, B. Alessandro ⁵⁷, R. Alfaro Molina ⁷³, A. Alici ^{11,25,52}, A. Alkin ³, J. Alme ²⁰, T. Alt ⁶⁹, L. Altenkamper ²⁰, I. Altsybeev ¹³⁶, C. Alves Garcia Prado ¹²¹, C. Andrei ⁸⁶, D. Andreou ³³, H.A. Andrews ¹¹⁰, A. Andronic ¹⁰⁶, V. Anguelov ¹⁰³, C. Anson ⁹⁶, T. Antičić ¹⁰⁷, F. Antinori ⁵⁵, P. Antonioli ⁵², R. Anwar ¹²⁴, L. Aphecetche ¹¹⁴, H. Appelshäuser ⁶⁹, S. Arcelli ²⁵, R. Arnaldi ⁵⁷, O.W. Arnold ^{104,34}, I.C. Arsene ¹⁹, M. Arslanbekov ¹⁰³, B. Audurier ¹¹⁴, A. Augustinus ³³, R. Averbeck ¹⁰⁶, M.D. Azmi ¹⁵, A. Badalà ⁵⁴, Y.W. Baek ^{59,77}, S. Bagnasco ⁵⁷, R. Bailhache ⁶⁹, R. Bala ¹⁰⁰, A. Baldissari ⁷⁴, M. Ball ⁴³, R.C. Baral ^{66,87}, A.M. Barbano ²⁴, R. Barbera ²⁶, F. Barile ^{51,31}, L. Barioglio ²⁴, G.G. Barnaföldi ¹⁴⁰, L.S. Barnby ⁹², V. Barret ¹³¹, P. Bartalini ⁷, K. Barth ³³, E. Bartsch ⁶⁹, M. Basile ²⁵, N. Bastid ¹³¹, S. Basu ¹³⁹, G. Batigne ¹¹⁴, B. Batyunya ⁷⁶, P.C. Batzing ¹⁹, I.G. Bearden ⁹⁰, H. Beck ¹⁰³, C. Bedda ⁶², N.K. Behera ⁵⁹, I. Belikov ¹³³, F. Bellini ^{25,33}, H. Bello Martinez ², R. Bellwied ¹²⁴, L.G.E. Beltran ¹²⁰, V. Belyaev ⁸², G. Bencedi ¹⁴⁰, S. Beole ²⁴, A. Bercuci ⁸⁶, Y. Berdnikov ⁹⁵, D. Berenyi ¹⁴⁰, R.A. Bertens ¹²⁷, D. Berzana ³³, L. Betev ³³, A. Bhasin ¹⁰⁰, I.R. Bhat ¹⁰⁰, A.K. Bhati ⁹⁸, B. Bhattacharjee ⁴², J. Bhom ¹¹⁸, A. Bianchi ²⁴, L. Bianchi ¹²⁴, N. Bianchi ⁴⁹, C. Bianchin ¹³⁹, J. Bielčík ³⁷, J. Bielčíková ⁹³, A. Bilandzic ^{34,104}, G. Biro ¹⁴⁰, R. Biswas ⁴, S. Biswas ⁴, J.T. Blair ¹¹⁹, D. Blau ⁸⁹, C. Blume ⁶⁹, G. Boca ¹³⁴, F. Bock ^{81,33,103}, A. Bogdanov ⁸², L. Boldizsár ¹⁴⁰, M. Bombara ³⁸, G. Bonomi ¹³⁵, M. Bonora ³³, J. Book ⁶⁹, H. Borel ⁷⁴, A. Borissov ^{103,17}, M. Borri ¹²⁶, E. Botta ²⁴, C. Bourjau ⁹⁰, L. Bratrud ⁶⁹, P. Braun-Munzinger ¹⁰⁶, M. Bregant ¹²¹, T.A. Broker ⁶⁹, M. Broz ³⁷, E.J. Brucken ⁴⁴, E. Bruna ⁵⁷, G.E. Bruno ^{33,31}, D. Budnikov ¹⁰⁸, H. Buesching ⁶⁹, S. Bufalino ²⁹, P. Buhler ¹¹³, P. Buncic ³³, O. Busch ¹³⁰, Z. Buthelezi ⁷⁵, J.B. Butt ¹⁴, J.T. Buxton ¹⁶, J. Cabala ¹¹⁶, D. Caffarri ^{33,91}, H. Caines ¹⁴¹, A. Caliva ^{62,106}, E. Calvo Villar ¹¹¹, P. Camerini ²³, A.A. Capon ¹¹³, F. Carena ³³, W. Carena ³³, F. Carnesecchi ^{25,11}, J. Castillo Castellanos ⁷⁴, A.J. Castro ¹²⁷, E.A.R. Casula ⁵³, C. Ceballos Sanchez ⁹, P. Cerello ⁵⁷, S. Chandra ¹³⁷, B. Chang ¹²⁵, S. Chapelard ³³, M. Chartier ¹²⁶, S. Chattopadhyay ¹³⁷, S. Chattopadhyay ¹⁰⁹, A. Chauvin ^{34,104}, C. Cheshkov ¹³², B. Cheynis ¹³², V. Chibante Barroso ³³, D.D. Chinellato ¹²², S. Cho ⁵⁹, P. Chochula ³³, M. Chojnacki ⁹⁰, S. Choudhury ¹³⁷, T. Chowdhury ¹³¹, P. Christakoglou ⁹¹, C.H. Christensen ⁹⁰, P. Christiansen ³², T. Chujo ¹³⁰, S.U. Chung ¹⁷, C. Cicalo ⁵³, L. Cifarelli ^{11,25}, F. Cindolo ⁵², J. Cleymans ⁹⁹, F. Colamaria ³¹, D. Colella ^{33,64,51}, A. Collu ⁸¹, M. Colocci ²⁵, M. Concas ^{57,ii}, G. Conesa Balbastre ⁸⁰, Z. Conesa del Valle ⁶⁰, M.E. Connors ^{141,iii}, J.G. Contreras ³⁷, T.M. Cormier ⁹⁴, Y. Corrales Morales ⁵⁷, I. Cortés Maldonado ², P. Cortese ³⁰, M.R. Cosentino ¹²³, F. Costa ³³, S. Costanza ¹³⁴, J. Crkovská ⁶⁰, P. Crochet ¹³¹, E. Cuautle ⁷¹, L. Cunqueiro ⁷⁰, T. Dahms ^{34,104}, A. Dainese ⁵⁵, M.C. Danisch ¹⁰³, A. Danu ⁶⁷, D. Das ¹⁰⁹, I. Das ¹⁰⁹, S. Das ⁴, A. Dash ⁸⁷, S. Dash ⁴⁶, S. De ^{47,121}, A. De Caro ²⁸, G. de Cataldo ⁵¹, C. de Conti ¹²¹, J. de Cuveland ⁴⁰, A. De Falco ²², D. De Gruttola ^{28,11}, N. De Marco ⁵⁷, S. De Pasquale ²⁸, R.D. De Souza ¹²², H.F. Degenhardt ¹²¹, A. Deisting ^{106,103}, A. Deloff ⁸⁵, C. Deplano ⁹¹, P. Dhankher ⁴⁶, D. Di Bari ³¹, A. Di Mauro ³³, P. Di Nezza ⁴⁹, B. Di Ruzza ⁵⁵, T. Dietel ⁹⁹, P. Dillenseger ⁶⁹, R. Divià ³³, Ø. Djuvsland ²⁰, A. Dobrin ³³, D. Domenicis Gimenez ¹²¹, B. Dönigus ⁶⁹, O. Dordic ¹⁹, L.V.R. Doremalen ⁶², A.K. Dubey ¹³⁷, A. Dubla ¹⁰⁶, L. Ducroux ¹³², A.K. Duggal ⁹⁸, M. Dukhishyam ⁸⁷, P. Dupieux ¹³¹, R.J. Ehlers ¹⁴¹, D. Elia ⁵¹, E. Endress ¹¹¹, H. Engel ⁶⁸, E. Epple ¹⁴¹, B. Erazmus ¹¹⁴, F. Erhardt ⁹⁷, B. Espagnon ⁶⁰, S. Esumi ¹³⁰, G. Eulisse ³³, J. Eum ¹⁷, D. Evans ¹¹⁰, S. Evdokimov ¹¹², L. Fabbietti ^{104,34}, J. Faivre ⁸⁰, A. Fantoni ⁴⁹, M. Fasel ^{94,81}, L. Feldkamp ⁷⁰, A. Feliciello ⁵⁷, G. Feofilov ¹³⁶, A. Fernández Téllez ², A. Ferretti ²⁴, A. Festanti ^{27,33}, V.J.G. Feuillard ^{74,131}, J. Figiel ¹¹⁸, M.A.S. Figueiredo ¹²¹, S. Filchagin ¹⁰⁸, D. Finogeev ⁶¹, F.M. Fionda ^{20,22}, M. Floris ³³, S. Foertsch ⁷⁵, P. Foka ¹⁰⁶, S. Fokin ⁸⁹, E. Fragiocomo ⁵⁸, A. Francescon ³³, A. Francisco ¹¹⁴, U. Frankenfeld ¹⁰⁶, G.G. Fronze ²⁴, U. Fuchs ³³, C. Furget ⁸⁰, A. Furs ⁶¹, M. Fusco Girard ²⁸, J.J. Gaardhøje ⁹⁰, M. Gagliardi ²⁴, A.M. Gago ¹¹¹, K. Gajdosova ⁹⁰, M. Gallio ²⁴, C.D. Galvan ¹²⁰, P. Ganoti ⁸⁴, C. Garabatos ¹⁰⁶, E. Garcia-Solis ¹², K. Garg ²⁶, C. Gargiulo ³³, P. Gasik ^{104,34}, E.F. Gauger ¹¹⁹, M.B. Gay Ducati ⁷², M. Germain ¹¹⁴, J. Ghosh ¹⁰⁹, P. Ghosh ¹³⁷, S.K. Ghosh ⁴, P. Gianotti ⁴⁹, P. Giubellino ^{106,33,57}, P. Giubilato ²⁷, E. Gladysz-Dziadus ¹¹⁸, P. Glässel ¹⁰³, D.M. Goméz Coral ⁷³, A. Gomez Ramirez ⁶⁸, A.S. Gonzalez ³³, P. González-Zamora ², S. Gorbunov ⁴⁰, L. Görlich ¹¹⁸, S. Gotovac ¹¹⁷, V. Grabski ⁷³, L.K. Graczykowski ¹³⁸, K.L. Graham ¹¹⁰, L. Greiner ⁸¹, A. Grelli ⁶², C. Grigoras ³³, V. Grigoriev ⁸², A. Grigoryan ¹, S. Grigoryan ⁷⁶, J.M. Gronefeld ¹⁰⁶, F. Grossa ²⁹, J.F. Grosse-Oetringhaus ³³, R. Grossi ¹⁰⁶, L. Gruber ¹¹³, F. Guber ⁶¹,

- R. Guernane ⁸⁰, B. Guerzoni ²⁵, K. Gulbrandsen ⁹⁰, T. Gunji ¹²⁹, A. Gupta ¹⁰⁰, R. Gupta ¹⁰⁰, I.B. Guzman ²,
 R. Haake ³³, C. Hadjidakis ⁶⁰, H. Hamagaki ⁸³, G. Hamar ¹⁴⁰, J.C. Hamon ¹³³, M.R. Haque ⁶², J.W. Harris ¹⁴¹,
 A. Harton ¹², H. Hassan ⁸⁰, D. Hatzifotiadou ^{11,52}, S. Hayashi ¹²⁹, S.T. Heckel ⁶⁹, E. Hellbär ⁶⁹,
 H. Helstrup ³⁵, A. Hergelegiu ⁸⁶, E.G. Hernandez ², G. Herrera Corral ¹⁰, F. Herrmann ⁷⁰, B.A. Hess ¹⁰²,
 K.F. Hetland ³⁵, H. Hillemanns ³³, C. Hills ¹²⁶, B. Hippolyte ¹³³, J. Hladky ⁶⁵, B. Hohlweger ¹⁰⁴, D. Horak ³⁷,
 S. Hornung ¹⁰⁶, R. Hosokawa ^{80,130}, P. Hristov ³³, C. Hughes ¹²⁷, T.J. Humanic ¹⁶, N. Hussain ⁴²,
 T. Hussain ¹⁵, D. Hutter ⁴⁰, D.S. Hwang ¹⁸, S.A. Iga Buitron ⁷¹, R. Ilkaev ¹⁰⁸, M. Inaba ¹³⁰, M. Ippolitov ^{82,89},
 M. Irfan ¹⁵, M.S. Islam ¹⁰⁹, M. Ivanov ¹⁰⁶, V. Ivanov ⁹⁵, V. Izucheev ¹¹², B. Jacak ⁸¹, N. Jacazio ²⁵,
 P.M. Jacobs ⁸¹, M.B. Jadhav ⁴⁶, J. Jadlovsky ¹¹⁶, S. Jaelani ⁶², C. Jahnke ³⁴, M.J. Jakubowska ¹³⁸,
 M.A. Janik ¹³⁸, P.H.S.Y. Jayarathna ¹²⁴, C. Jena ⁸⁷, S. Jena ¹²⁴, M. Jercic ⁹⁷, R.T. Jimenez Bustamante ¹⁰⁶,
 P.G. Jones ¹¹⁰, A. Jusko ¹¹⁰, P. Kalinak ⁶⁴, A. Kalweit ³³, J.H. Kang ¹⁴², V. Kaplin ⁸², S. Kar ¹³⁷,
 A. Karasu Uysal ⁷⁹, O. Karavichev ⁶¹, T. Karavicheva ⁶¹, L. Karayan ^{106,103}, P. Karczmarczyk ³³,
 E. Karpechev ⁶¹, U. Kebschull ⁶⁸, R. Keidel ¹⁴³, D.L.D. Keijdener ⁶², M. Keil ³³, B. Ketzer ⁴³, Z. Khabanova ⁹¹,
 P. Khan ¹⁰⁹, S.A. Khan ¹³⁷, A. Khanzadeev ⁹⁵, Y. Kharlov ¹¹², A. Khatun ¹⁵, A. Khuntia ⁴⁷,
 M.M. Kielbowicz ¹¹⁸, B. Kileng ³⁵, B. Kim ¹³⁰, D. Kim ¹⁴², D.J. Kim ¹²⁵, H. Kim ¹⁴², J.S. Kim ⁴¹, J. Kim ¹⁰³,
 M. Kim ⁵⁹, M. Kim ¹⁴², S. Kim ¹⁸, T. Kim ¹⁴², S. Kirsch ⁴⁰, I. Kisel ⁴⁰, S. Kiselev ⁶³, A. Kisiel ¹³⁸, G. Kiss ¹⁴⁰,
 J.L. Klay ⁶, C. Klein ⁶⁹, J. Klein ³³, C. Klein-Bösing ⁷⁰, S. Klewin ¹⁰³, A. Kluge ³³, M.L. Knichel ^{103,33},
 A.G. Knospe ¹²⁴, C. Kobdaj ¹¹⁵, M. Kofarago ¹⁴⁰, M.K. Köhler ¹⁰³, T. Kollegger ¹⁰⁶, V. Kondratiev ¹³⁶,
 N. Kondratyeva ⁸², E. Kondratyuk ¹¹², A. Konevskikh ⁶¹, M. Konyushikhin ¹³⁹, M. Kopcik ¹¹⁶, M. Kour ¹⁰⁰,
 C. Kouzinopoulos ³³, O. Kovalenko ⁸⁵, V. Kovalenko ¹³⁶, M. Kowalski ¹¹⁸, G. Koyithatta Meethaleveedu ⁴⁶,
 I. Králik ⁶⁴, A. Kravčáková ³⁸, L. Kreis ¹⁰⁶, M. Krivda ^{110,64}, F. Krizek ⁹³, E. Kryshen ⁹⁵, M. Krzewicki ⁴⁰,
 A.M. Kubera ¹⁶, V. Kučera ⁹³, C. Kuhn ¹³³, P.G. Kuijer ⁹¹, A. Kumar ¹⁰⁰, J. Kumar ⁴⁶, L. Kumar ⁹⁸, S. Kumar ⁴⁶,
 S. Kundu ⁸⁷, P. Kurashvili ⁸⁵, A. Kurepin ⁶¹, A.B. Kurepin ⁶¹, A. Kuryakin ¹⁰⁸, S. Kushpil ⁹³, M.J. Kweon ⁵⁹,
 Y. Kwon ¹⁴², S.L. La Pointe ⁴⁰, P. La Rocca ²⁶, C. Lagana Fernandes ¹²¹, Y.S. Lai ⁸¹, I. Lakomov ³³,
 R. Langoy ³⁹, K. Lapidus ¹⁴¹, C. Lara ⁶⁸, A. Lardeux ^{74,19}, A. Lattuca ²⁴, E. Laudi ³³, R. Lavicka ³⁷, R. Lea ²³,
 L. Leardini ¹⁰³, S. Lee ¹⁴², F. Lehas ⁹¹, S. Lehner ¹¹³, J. Lehrbach ⁴⁰, R.C. Lemmon ⁹², V. Lenti ⁵¹,
 E. Leogrande ⁶², I. León Monzón ¹²⁰, P. Lévai ¹⁴⁰, X. Li ¹³, J. Lien ³⁹, R. Lietava ¹¹⁰, B. Lim ¹⁷, S. Lindal ¹⁹,
 V. Lindenstruth ⁴⁰, S.W. Lindsay ¹²⁶, C. Lippmann ¹⁰⁶, M.A. Lisa ¹⁶, V. Litichevskyi ⁴⁴, W.J. Llope ¹³⁹,
 D.F. Lodato ⁶², P.I. Loenne ²⁰, V. Loginov ⁸², C. Loizides ⁸¹, P. Loncar ¹¹⁷, X. Lopez ¹³¹, E. López Torres ⁹,
 A. Lowe ¹⁴⁰, P. Luettig ⁶⁹, J.R. Luhder ⁷⁰, M. Lunardon ²⁷, G. Luparello ^{58,23}, M. Lupi ³³, T.H. Lutz ¹⁴¹,
 A. Maevskaia ⁶¹, M. Mager ³³, S. Mahajan ¹⁰⁰, S.M. Mahmood ¹⁹, A. Maire ¹³³, R.D. Majka ¹⁴¹,
 M. Malaev ⁹⁵, L. Malinina ^{76,iv}, D. Mal'Kevich ⁶³, P. Malzacher ¹⁰⁶, A. Mamonov ¹⁰⁸, V. Manko ⁸⁹,
 F. Manso ¹³¹, V. Manzari ⁵¹, Y. Mao ⁷, M. Marchisone ^{75,128}, J. Mareš ⁶⁵, G.V. Margagliotti ²³, A. Margotti ⁵²,
 J. Margutti ⁶², A. Marín ¹⁰⁶, C. Markert ¹¹⁹, M. Marquard ⁶⁹, N.A. Martin ¹⁰⁶, P. Martinengo ³³,
 J.A.L. Martinez ⁶⁸, M.I. Martínez ², G. Martínez García ¹¹⁴, M. Martinez Pedreira ³³, S. Masciocchi ¹⁰⁶,
 M. Masera ²⁴, A. Masoni ⁵³, E. Masson ¹¹⁴, A. Mastroserio ⁵¹, A.M. Mathis ^{104,34}, P.F.T. Matuoka ¹²¹,
 A. Matyja ¹²⁷, C. Mayer ¹¹⁸, J. Mazer ¹²⁷, M. Mazzilli ³¹, M.A. Mazzoni ⁵⁶, F. Meddi ²¹, Y. Melikyan ⁸²,
 A. Menchaca-Rocha ⁷³, E. Meninno ²⁸, J. Mercado Pérez ¹⁰³, M. Meres ³⁶, S. Mhlanga ⁹⁹, Y. Miake ¹³⁰,
 M.M. Mieskolainen ⁴⁴, D.L. Mihaylov ¹⁰⁴, K. Mikhaylov ^{63,76}, J. Milosevic ¹⁹, A. Mischke ⁶², A.N. Mishra ⁴⁷,
 D. Miśkowiec ¹⁰⁶, J. Mitra ¹³⁷, C.M. Mitu ⁶⁷, N. Mohammadi ⁶², B. Mohanty ⁸⁷, M. Mohisin Khan ^{15,v},
 D.A. Moreira De Godoy ⁷⁰, L.A.P. Moreno ², S. Moretto ²⁷, A. Morreale ¹¹⁴, A. Morsch ³³, V. Muccifora ⁴⁹,
 E. Mudnic ¹¹⁷, D. Mühlheim ⁷⁰, S. Muhuri ¹³⁷, M. Mukherjee ⁴, J.D. Mulligan ¹⁴¹, M.G. Munhoz ¹²¹,
 K. Münning ⁴³, R.H. Munzer ⁶⁹, H. Murakami ¹²⁹, S. Murray ⁷⁵, L. Musa ³³, J. Musinsky ⁶⁴, C.J. Myers ¹²⁴,
 J.W. Myrcha ¹³⁸, D. Nag ⁴, B. Naik ⁴⁶, R. Nair ⁸⁵, B.K. Nandi ⁴⁶, R. Nania ^{52,11}, E. Nappi ⁵¹, A. Narayan ⁴⁶,
 M.U. Naru ¹⁴, H. Natal da Luz ¹²¹, C. Nattrass ¹²⁷, S.R. Navarro ², K. Nayak ⁸⁷, R. Nayak ⁴⁶, T.K. Nayak ¹³⁷,
 S. Nazarenko ¹⁰⁸, A. Nedosekin ⁶³, R.A. Negrao De Oliveira ³³, L. Nellen ⁷¹, S.V. Nesbo ³⁵, F. Ng ¹²⁴,
 M. Nicassio ¹⁰⁶, M. Niculescu ⁶⁷, J. Niedziela ^{138,33}, B.S. Nielsen ⁹⁰, S. Nikolaev ⁸⁹, S. Nikulin ⁸⁹,
 V. Nikulin ⁹⁵, F. Noferini ^{11,52}, P. Nomokonov ⁷⁶, G. Nooren ⁶², J.C.C. Noris ², J. Norman ¹²⁶, A. Nyanin ⁸⁹,
 J. Nystrand ²⁰, H. Oeschler ^{17,103,i}, S. Oh ¹⁴¹, A. Ohlson ^{33,103}, T. Okubo ⁴⁵, L. Olah ¹⁴⁰, J. Oleniacz ¹³⁸,
 A.C. Oliveira Da Silva ¹²¹, M.H. Oliver ¹⁴¹, J. Onderwaater ¹⁰⁶, C. Oppedisano ⁵⁷, R. Orava ⁴⁴, M. Oravec ¹¹⁶,
 A. Ortiz Velasquez ⁷¹, A. Oskarsson ³², J. Otwinowski ¹¹⁸, K. Oyama ⁸³, Y. Pachmayer ¹⁰³, V. Pacik ⁹⁰,
 D. Pagano ¹³⁵, P. Pagano ²⁸, G. Paić ⁷¹, P. Palni ⁷, J. Pan ¹³⁹, A.K. Pandey ⁴⁶, S. Panebianco ⁷⁴, V. Papikyan ¹,

- G.S. Pappalardo 54, P. Pareek 47, J. Park 59, S. Parmar 98, A. Passfeld 70, S.P. Pathak 124, R.N. Patra 137,
 B. Paul 57, H. Pei 7, T. Peitzmann 62, X. Peng 7, L.G. Pereira Da Costa 74, D. Peresunko 89, 82,
 E. Perez Lezama 69, V. Peskov 69, Y. Pestov 5, V. Petráček 37, V. Petrov 112, M. Petrovici 86, C. Petta 26,
 R.P. Pezzi 72, S. Piano 58, M. Pikna 36, P. Pillot 114, L.O.D.L. Pimentel 90, O. Pinazza 52, 33, L. Pinsky 124,
 D.B. Piyarathna 124, M. Płoskoń 81, M. Planinic 97, F. Pliquet 69, J. Pluta 138, S. Pochybova 140,
 P.L.M. Podesta-Lerma 120, M.G. Poghosyan 94, B. Polichtchouk 112, N. Poljak 97, W. Poonsawat 115, A. Pop 86,
 H. Poppenborg 70, S. Porteboeuf-Houssais 131, V. Pozdniakov 76, S.K. Prasad 4, R. Preghenella 52, F. Prino 57,
 C.A. Pruneau 139, I. Pshenichnov 61, M. Puccio 24, G. Puddu 22, P. Pujahari 139, V. Punin 108, J. Putschke 139,
 S. Raha 4, S. Rajput 100, J. Rak 125, A. Rakotozafindrabe 74, L. Ramello 30, F. Rami 133, D.B. Rana 124,
 R. Raniwala 101, S. Raniwala 101, S.S. Räsänen 44, B.T. Rascanu 69, D. Rathee 98, V. Ratza 43, I. Ravasenga 29,
 K.F. Read 127, 94, K. Redlich 85, vi, A. Rehman 20, P. Reichelt 69, F. Reidt 33, X. Ren 7, R. Renfordt 69,
 A.R. Reolon 49, A. Reshetin 61, K. Reygers 103, V. Riabov 95, R.A. Ricci 50, T. Richert 32, M. Richter 19,
 P. Riedler 33, W. Riegler 33, F. Riggi 26, C. Ristea 67, M. Rodríguez Cahuantzi 2, K. Røed 19, E. Rogochaya 76,
 D. Rohr 33, 40, D. Röhrich 20, P.S. Rokita 138, F. Ronchetti 49, E.D. Rosas 71, P. Rosnet 131, A. Rossi 27, 55,
 A. Rotondi 134, F. Roukoutakis 84, A. Roy 47, C. Roy 133, P. Roy 109, O.V. Rueda 71, R. Rui 23,
 B. Rumyantsev 76, A. Rustamov 88, E. Ryabinkin 89, Y. Ryabov 95, A. Rybicki 118, S. Saarinen 44, S. Sadhu 137,
 S. Sadovsky 112, K. Šafařík 33, S.K. Saha 137, B. Sahlmuller 69, B. Sahoo 46, P. Sahoo 47, R. Sahoo 47,
 S. Sahoo 66, P.K. Sahu 66, J. Saini 137, S. Sakai 130, M.A. Saleh 139, J. Salzwedel 16, S. Sambyal 100,
 V. Samsonov 95, 82, A. Sandoval 73, D. Sarkar 137, N. Sarkar 137, P. Sarma 42, M.H.P. Sas 62, E. Scapparone 52,
 F. Scarlassara 27, B. Schaefer 94, R.P. Scharenberg 105, H.S. Scheid 69, C. Schiaua 86, R. Schicker 103,
 C. Schmidt 106, H.R. Schmidt 102, M.O. Schmidt 103, M. Schmidt 102, N.V. Schmidt 94, 69, J. Schukraft 33,
 Y. Schutz 33, 133, K. Schwarz 106, K. Schweda 106, G. Scioli 25, E. Scomparin 57, M. Šefčík 38, J.E. Seger 96,
 Y. Sekiguchi 129, D. Sekihata 45, I. Selyuzhenkov 106, 82, K. Senosi 75, S. Senyukov 3, 133, 33, E. Serradilla 73,
 P. Sett 46, A. Sevcenco 67, A. Shabanov 61, A. Shabetai 114, R. Shahoyan 33, W. Shaikh 109, A. Shangaraev 112,
 A. Sharma 98, A. Sharma 100, M. Sharma 100, M. Sharma 100, N. Sharma 98, 127, A.I. Sheikh 137, K. Shigaki 45,
 Q. Shou 7, K. Shtejer 9, 24, Y. Sibiriak 89, S. Siddhanta 53, K.M. Sielewicz 33, T. Siemarczuk 85, S. Silaeva 89,
 D. Silvermyr 32, C. Silvestre 80, G. Simatovic 97, G. Simonetti 33, R. Singaraju 137, R. Singh 87, V. Singhal 137,
 T. Sinha 109, B. Sitar 36, M. Sitta 30, T.B. Skaali 19, M. Slupecki 125, N. Smirnov 141, R.J.M. Snellings 62,
 T.W. Snellman 125, J. Song 17, M. Song 142, F. Soramel 27, S. Sorensen 127, F. Sozzi 106, E. Spiriti 49,
 I. Sputowska 118, B.K. Srivastava 105, J. Stachel 103, I. Stan 67, P. Stankus 94, E. Stenlund 32, D. Stocco 114,
 M.M. Storetvedt 35, P. Strmen 36, A.A.P. Suaide 121, T. Sugitate 45, C. Suire 60, M. Suleymanov 14,
 M. Suljic 23, R. Sultanov 63, M. Šumbera 93, S. Sumowidagdo 48, K. Suzuki 113, S. Swain 66, A. Szabo 36,
 I. Szarka 36, U. Tabassam 14, J. Takahashi 122, G.J. Tambave 20, N. Tanaka 130, M. Tarhini 60, M. Tariq 15,
 M.G. Tarzila 86, A. Tauro 33, G. Tejeda Muñoz 2, A. Telesca 33, K. Terasaki 129, C. Terrevoli 27, B. Teyssier 132,
 D. Thakur 47, S. Thakur 137, D. Thomas 119, F. Thoresen 90, R. Tieulent 132, A. Tikhonov 61, A.R. Timmins 124,
 A. Toia 69, S.R. Torres 120, S. Tripathy 47, S. Trogolo 24, G. Trombetta 31, L. Tropp 38, V. Trubnikov 3,
 W.H. Trzaska 125, B.A. Trzeciak 62, T. Tsuji 129, A. Tumkin 108, R. Turrisi 55, T.S. Tveter 19, K. Ullaland 20,
 E.N. Umaka 124, A. Uras 132, G.L. Usai 22, A. Utrobicic 97, M. Vala 116, 64, J. Van Der Maarel 62,
 J.W. Van Hoorné 33, M. van Leeuwen 62, T. Vanat 93, P. Vande Vyvre 33, D. Varga 140, A. Vargas 2,
 M. Vargyas 125, R. Varma 46, M. Vasileiou 84, A. Vasiliev 89, A. Vauthier 80, O. Vázquez Doce 104, 34,
 V. Vechernin 136, A.M. Veen 62, A. Velure 20, E. Vercellin 24, S. Vergara Limón 2, R. Vernet 8, R. Vértesi 140,
 L. Vickovic 117, S. Vigolo 62, J. Viinikainen 125, Z. Vilakazi 128, O. Villalobos Baillie 110, A. Villatoro Tello 2,
 A. Vinogradov 89, L. Vinogradov 136, T. Virgili 28, V. Vislavicius 32, A. Vodopyanov 76, M.A. Völkl 103, 102,
 K. Voloshin 63, S.A. Voloshin 139, G. Volpe 31, B. von Haller 33, I. Vorobyev 104, 34, D. Voscek 116,
 D. Vranic 33, 106, J. Vrláková 38, B. Wagner 20, H. Wang 62, M. Wang 7, D. Watanabe 130, Y. Watanabe 129, 130,
 M. Weber 113, S.G. Weber 106, D.F. Weiser 103, S.C. Wenzel 33, J.P. Wessels 70, U. Westerhoff 70,
 A.M. Whitehead 99, J. Wiechula 69, J. Wikne 19, G. Wilk 85, J. Wilkinson 103, 52, G.A. Willems 33, 70,
 M.C.S. Williams 52, E. Willsher 110, B. Windelband 103, W.E. Witt 127, S. Yalcin 79, K. Yamakawa 45,
 P. Yang 7, S. Yano 45, Z. Yin 7, H. Yokoyama 130, 80, I.-K. Yoo 17, J.H. Yoon 59, V. Yurchenko 3, V. Zaccolo 57,
 A. Zaman 14, C. Zampolli 33, H.J.C. Zanolli 121, N. Zardoshti 110, A. Zarochentsev 136, P. Závada 65,
 N. Zaviyalov 108, H. Zbroszczyk 138, M. Zhalov 95, H. Zhang 20, 7, X. Zhang 7, Y. Zhang 62, C. Zhang

Z. Zhang ^{7,131}, C. Zhao ¹⁹, N. Zhigareva ⁶³, D. Zhou ⁷, Y. Zhou ⁹⁰, Z. Zhou ²⁰, H. Zhu ²⁰, J. Zhu ⁷, A. Zichichi ^{25,11}, A. Zimmermann ¹⁰³, M.B. Zimmermann ³³, G. Zinovjev ³, J. Zmeskal ¹¹³, S. Zou ⁷

¹ A.I. Alikhanyan National Science Laboratory (Yerevan Physics Institute) Foundation, Yerevan, Armenia

² Benemérita Universidad Autónoma de Puebla, Puebla, Mexico

³ Bogolyubov Institute for Theoretical Physics, Kiev, Ukraine

⁴ Bose Institute, Department of Physics and Centre for Astroparticle Physics and Space Science (CAPSS), Kolkata, India

⁵ Budker Institute for Nuclear Physics, Novosibirsk, Russia

⁶ California Polytechnic State University, San Luis Obispo, CA, United States

⁷ Central China Normal University, Wuhan, China

⁸ Centre de Calcul de l'IN2P3, Villeurbanne, Lyon, France

⁹ Centro de Aplicaciones Tecnológicas y Desarrollo Nuclear (CEADEN), Havana, Cuba

¹⁰ Centro de Investigación y de Estudios Avanzados (CINVESTAV), Mexico City and Mérida, Mexico

¹¹ Centro Fermi – Museo Storico della Fisica e Centro Studi e Ricerche “Enrico Fermi”, Rome, Italy

¹² Chicago State University, Chicago, IL, United States

¹³ China Institute of Atomic Energy, Beijing, China

¹⁴ COMSATS Institute of Information Technology (CIIT), Islamabad, Pakistan

¹⁵ Department of Physics, Aligarh Muslim University, Aligarh, India

¹⁶ Department of Physics, Ohio State University, Columbus, OH, United States

¹⁷ Department of Physics, Pusan National University, Pusan, Republic of Korea

¹⁸ Department of Physics, Sejong University, Seoul, Republic of Korea

¹⁹ Department of Physics, University of Oslo, Oslo, Norway

²⁰ Department of Physics and Technology, University of Bergen, Bergen, Norway

²¹ Dipartimento di Fisica dell’Università ‘La Sapienza’ and Sezione INFN, Rome, Italy

²² Dipartimento di Fisica dell’Università and Sezione INFN, Cagliari, Italy

²³ Dipartimento di Fisica dell’Università and Sezione INFN, Trieste, Italy

²⁴ Dipartimento di Fisica dell’Università and Sezione INFN, Turin, Italy

²⁵ Dipartimento di Fisica e Astronomia dell’Università and Sezione INFN, Bologna, Italy

²⁶ Dipartimento di Fisica e Astronomia dell’Università and Sezione INFN, Catania, Italy

²⁷ Dipartimento di Fisica e Astronomia dell’Università and Sezione INFN, Padova, Italy

²⁸ Dipartimento di Fisica ‘E.R. Caianiello’ dell’Università and Gruppo Collegato INFN, Salerno, Italy

²⁹ Dipartimento DISAT del Politecnico and Sezione INFN, Turin, Italy

³⁰ Dipartimento di Scienze e Innovazione Tecnologica dell’Università del Piemonte Orientale and INFN Sezione di Torino, Alessandria, Italy

³¹ Dipartimento Interateneo di Fisica ‘M. Merlin’ and Sezione INFN, Bari, Italy

³² Division of Experimental High Energy Physics, University of Lund, Lund, Sweden

³³ European Organization for Nuclear Research (CERN), Geneva, Switzerland

³⁴ Excellence Cluster Universe, Technische Universität München, Munich, Germany

³⁵ Faculty of Engineering, Bergen University College, Bergen, Norway

³⁶ Faculty of Mathematics, Physics and Informatics, Comenius University, Bratislava, Slovakia

³⁷ Faculty of Nuclear Sciences and Physical Engineering, Czech Technical University in Prague, Prague, Czech Republic

³⁸ Faculty of Science, P.J. Šafárik University, Košice, Slovakia

³⁹ Faculty of Technology, Buskerud and Vestfold University College, Tønsberg, Norway

⁴⁰ Frankfurt Institute for Advanced Studies, Johann Wolfgang Goethe-Universität Frankfurt, Frankfurt, Germany

⁴¹ Gangneung-Wonju National University, Gangneung, Republic of Korea

⁴² Gauhati University, Department of Physics, Guwahati, India

⁴³ Helmholtz-Institut für Strahlen- und Kernphysik, Rheinische Friedrich-Wilhelms-Universität Bonn, Bonn, Germany

⁴⁴ Helsinki Institute of Physics (HIP), Helsinki, Finland

⁴⁵ Hiroshima University, Hiroshima, Japan

⁴⁶ Indian Institute of Technology Bombay (IIT), Mumbai, India

⁴⁷ Indian Institute of Technology Indore, Indore, India

⁴⁸ Indonesian Institute of Sciences, Jakarta, Indonesia

⁴⁹ INFN, Laboratori Nazionali di Frascati, Frascati, Italy

⁵⁰ INFN, Laboratori Nazionali di Legnaro, Legnaro, Italy

⁵¹ INFN, Sezione di Bari, Bari, Italy

⁵² INFN, Sezione di Bologna, Bologna, Italy

⁵³ INFN, Sezione di Cagliari, Cagliari, Italy

⁵⁴ INFN, Sezione di Catania, Catania, Italy

⁵⁵ INFN, Sezione di Padova, Padova, Italy

⁵⁶ INFN, Sezione di Roma, Roma, Italy

⁵⁷ INFN, Sezione di Torino, Turin, Italy

⁵⁸ INFN, Sezione di Trieste, Trieste, Italy

⁵⁹ Inha University, Incheon, Republic of Korea

⁶⁰ Institut de Physique Nucléaire d’Orsay (IPNO), Université Paris-Sud, CNRS-IN2P3, Orsay, France

⁶¹ Institute for Nuclear Research, Academy of Sciences, Moscow, Russia

⁶² Institute for Subatomic Physics of Utrecht University, Utrecht, Netherlands

⁶³ Institute for Theoretical and Experimental Physics, Moscow, Russia

⁶⁴ Institute of Experimental Physics, Slovak Academy of Sciences, Košice, Slovakia

⁶⁵ Institute of Physics, Academy of Sciences of the Czech Republic, Prague, Czech Republic

⁶⁶ Institute of Physics, Bhubaneswar, India

⁶⁷ Institute of Space Science (ISS), Bucharest, Romania

⁶⁸ Institut für Informatik, Johann Wolfgang Goethe-Universität Frankfurt, Frankfurt, Germany

⁶⁹ Institut für Kernphysik, Johann Wolfgang Goethe-Universität Frankfurt, Frankfurt, Germany

⁷⁰ Institut für Kernphysik, Westfälische Wilhelms-Universität Münster, Münster, Germany

⁷¹ Instituto de Ciencias Nucleares, Universidad Nacional Autónoma de México, Mexico City, Mexico

⁷² Instituto de Física, Universidade Federal do Rio Grande do Sul (UFRGS), Porto Alegre, Brazil

⁷³ Instituto de Física, Universidad Nacional Autónoma de México, Mexico City, Mexico

⁷⁴ IRFU, CEA, Université Paris-Saclay, Saclay, France

⁷⁵ iThemba LABS, National Research Foundation, Somerset West, South Africa

- ⁷⁶ Joint Institute for Nuclear Research (JINR), Dubna, Russia
⁷⁷ Konkuk University, Seoul, Republic of Korea
⁷⁸ Korea Institute of Science and Technology Information, Daejeon, Republic of Korea
⁷⁹ KTO Karatay University, Konya, Turkey
⁸⁰ Laboratoire de Physique Subatomique et de Cosmologie, Université Grenoble-Alpes, CNRS-IN2P3, Grenoble, France
⁸¹ Lawrence Berkeley National Laboratory, Berkeley, CA, United States
⁸² Moscow Engineering Physics Institute, Moscow, Russia
⁸³ Nagasaki Institute of Applied Science, Nagasaki, Japan
⁸⁴ National and Kapodistrian University of Athens, Physics Department, Athens, Greece
⁸⁵ National Centre for Nuclear Studies, Warsaw, Poland
⁸⁶ National Institute for Physics and Nuclear Engineering, Bucharest, Romania
⁸⁷ National Institute of Science Education and Research, HBNI, Jatni, India
⁸⁸ National Nuclear Research Center, Baku, Azerbaijan
⁸⁹ National Research Centre Kurchatov Institute, Moscow, Russia
⁹⁰ Niels Bohr Institute, University of Copenhagen, Copenhagen, Denmark
⁹¹ Nikhef, Nationaal instituut voor subatomaire fysica, Amsterdam, Netherlands
⁹² Nuclear Physics Group, STFC Daresbury Laboratory, Daresbury, United Kingdom
⁹³ Nuclear Physics Institute, Academy of Sciences of the Czech Republic, Řež u Prahy, Czech Republic
⁹⁴ Oak Ridge National Laboratory, Oak Ridge, TN, United States
⁹⁵ Petersburg Nuclear Physics Institute, Gatchina, Russia
⁹⁶ Physics Department, Creighton University, Omaha, NE, United States
⁹⁷ Physics Department, Faculty of Science, University of Zagreb, Zagreb, Croatia
⁹⁸ Physics Department, Panjab University, Chandigarh, India
⁹⁹ Physics Department, University of Cape Town, Cape Town, South Africa
¹⁰⁰ Physics Department, University of Jammu, Jammu, India
¹⁰¹ Physics Department, University of Rajasthan, Jaipur, India
¹⁰² Physikalisches Institut, Eberhard Karls Universität Tübingen, Tübingen, Germany
¹⁰³ Physikalisches Institut, Ruprecht-Karls-Universität Heidelberg, Heidelberg, Germany
¹⁰⁴ Physik Department, Technische Universität München, Munich, Germany
¹⁰⁵ Purdue University, West Lafayette, IN, United States
¹⁰⁶ Research Division and ExtreMe Matter Institute EMMI, GSI Helmholtzzentrum für Schwerionenforschung GmbH, Darmstadt, Germany
¹⁰⁷ Rudjer Bošković Institute, Zagreb, Croatia
¹⁰⁸ Russian Federal Nuclear Center (VNIIEF), Sarov, Russia
¹⁰⁹ Saha Institute of Nuclear Physics, Kolkata, India
¹¹⁰ School of Physics and Astronomy, University of Birmingham, Birmingham, United Kingdom
¹¹¹ Sección Física, Departamento de Ciencias, Pontificia Universidad Católica del Perú, Lima, Peru
¹¹² SSC IHEP of NRC Kurchatov Institute, Protvino, Russia
¹¹³ Stefan Meyer Institut für Subatomare Physik (SMI), Vienna, Austria
¹¹⁴ SUBATECH, IMT Atlantique, Université de Nantes, CNRS-IN2P3, Nantes, France
¹¹⁵ Suranaree University of Technology, Nakhon Ratchasima, Thailand
¹¹⁶ Technical University of Košice, Košice, Slovakia
¹¹⁷ Technical University of Split FESB, Split, Croatia
¹¹⁸ The Henryk Niewodniczanski Institute of Nuclear Physics, Polish Academy of Sciences, Cracow, Poland
¹¹⁹ The University of Texas at Austin, Physics Department, Austin, TX, United States
¹²⁰ Universidad Autónoma de Sinaloa, Culiacán, Mexico
¹²¹ Universidade de São Paulo (USP), São Paulo, Brazil
¹²² Universidade Estadual de Campinas (UNICAMP), Campinas, Brazil
¹²³ Universidade Federal do ABC, Santo André, Brazil
¹²⁴ University of Houston, Houston, TX, United States
¹²⁵ University of Jyväskylä, Jyväskylä, Finland
¹²⁶ University of Liverpool, Liverpool, United Kingdom
¹²⁷ University of Tennessee, Knoxville, TN, United States
¹²⁸ University of the Witwatersrand, Johannesburg, South Africa
¹²⁹ University of Tokyo, Tokyo, Japan
¹³⁰ University of Tsukuba, Tsukuba, Japan
¹³¹ Université Clermont Auvergne, CNRS/IN2P3, LPC, Clermont-Ferrand, France
¹³² Université de Lyon, Université Lyon 1, CNRS/IN2P3, IPN-Lyon, Villeurbanne, Lyon, France
¹³³ Université de Strasbourg, CNRS, IPHC UMR 7118, F-67000 Strasbourg, France
¹³⁴ Università degli Studi di Pavia, Pavia, Italy
¹³⁵ Università di Brescia, Brescia, Italy
¹³⁶ V. Fock Institute for Physics, St. Petersburg State University, St. Petersburg, Russia
¹³⁷ Variable Energy Cyclotron Centre, Kolkata, India
¹³⁸ Warsaw University of Technology, Warsaw, Poland
¹³⁹ Wayne State University, Detroit, MI, United States
¹⁴⁰ Wigner Research Centre for Physics, Hungarian Academy of Sciences, Budapest, Hungary
¹⁴¹ Yale University, New Haven, CT, United States
¹⁴² Yonsei University, Seoul, Republic of Korea
¹⁴³ Zentrum für Technologietransfer und Telekommunikation (ZTT), Fachhochschule Worms, Worms, Germany

ⁱ Deceased.ⁱⁱ Dipartimento DET del Politecnico di Torino, Turin, Italy.ⁱⁱⁱ Georgia State University, Atlanta, Georgia, United States.^{iv} M.V. Lomonosov Moscow State University, D.V. Skobeltsyn Institute of Nuclear, Physics, Moscow, Russia.^v Department of Applied Physics, Aligarh Muslim University, Aligarh, India.^{vi} Institute of Theoretical Physics, University of Wroclaw, Poland.